analytical chemistry

pubs.acs.org/ac Article

Double Emulsion Picoreactors for High-Throughput Single-Cell Encapsulation and Phenotyping via FACS

Kara K. Brower,◆ Margarita Khariton,◆ Peter H. Suzuki, Chris Still, II, Gaeun Kim, Suzanne G. K. Calhoun, Lei S. Qi, Bo Wang,* and Polly M. Fordyce*

Cite This: *Anal. Chem.* 2020, 92, 13262−13270 Read Online

ACCESS | Metrics & More | Article Recommendations | Supporting Information

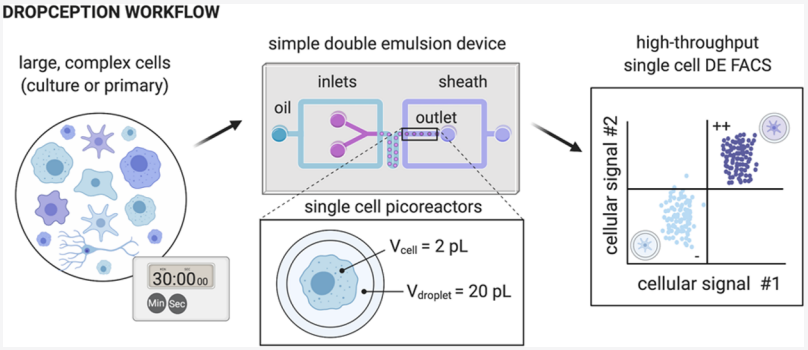

ABSTRACT: In the past five years, droplet microfluidic techniques have unlocked new opportunities for the high-throughput genome-wide analysis of single cells, transforming our understanding of cellular diversity and function. However, the field lacks an accessible method to screen and sort droplets based on cellular phenotype upstream of genetic analysis, particularly for large and complex cells. To meet this need, we developed Dropception, a robust, easy-to-use workflow for precise single-cell encapsulation into picoliter-scale double emulsion droplets compatible with high-throughput screening via fluorescence-activated cell sorting (FACS). We demonstrate the capabilities of this method by encapsulating five standardized mammalian cell lines of varying sizes and morphologies as well as a heterogeneous cell mixture of a whole dissociated flatworm (5−25 μm in diameter) within highly monodisperse double emulsions (35 μm in diameter). We optimize for preferential encapsulation of single cells with extremely low multiple-cell loading events (<2% of cell-containing droplets), thereby allowing direct linkage of cellular phenotype to genotype. Across all cell lines, cell loading efficiency approaches the theoretical limit with no observable bias by cell size. FACS measurements reveal the ability to discriminate empty droplets from those containing cells with good agreement to single-cell occupancies quantified via microscopy, establishing robust droplet screening at single-cell resolution. High-throughput FACS screening of cellular picoreactors has the potential to shift the landscape of single-cell droplet microfluidics by expanding the repertoire of current nucleic acid droplet assays to include functional phenotyping.

INTRODUCTION

The last decade has yielded an exponential rise in new methods to analyze single cells,[1,2] revealing critical insights into cellular diversity,[3−5] tissue organization,[6,7] and organism development.[8] In particular, droplet microfluidics has emerged as a powerful class of single-cell isolation techniques due to its unprecedented scale (0.1−10 M droplets per run), throughput (0.1−30 kHz generation rate), and efficiency ($0.10−0.50 per cell).[9−11] Novel droplet assays have enabled thousands of single cells to be profiled by genome,[12] epigenome,[13] transcriptome,[3,4,14] or proteome,[15,16] leading to the generation of the first whole-organism cell atlases.[17−19] Due to their ease of operation and low barrier to entry, open-source droplet technologies (e.g., DropSeq,[3] InDrops[4]) have been adopted by specialists and nonspecialists alike with commercial droplet platforms (e.g., 10X Genomics[14]) achieving widespread market penetration in research laboratories worldwide.[9]

Despite these advances, single-cell droplet techniques remain fundamentally limited in their ability to easily screen droplets based on cellular presence and phenotypic signals.[10] This capability would enable new opportunities for single-cell analysis. First, isolating and sequencing only those droplets containing cells via the use of a cellular stain or nonspecific viability dye would dramatically lower costs[9] while increasing

Received: June 11, 2020
Accepted: September 9, 2020
Published: September 9, 2020

https://dx.doi.org/10.1021/acs.analchem.0c02499
Anal. Chem. 2020, 92, 13262−13270

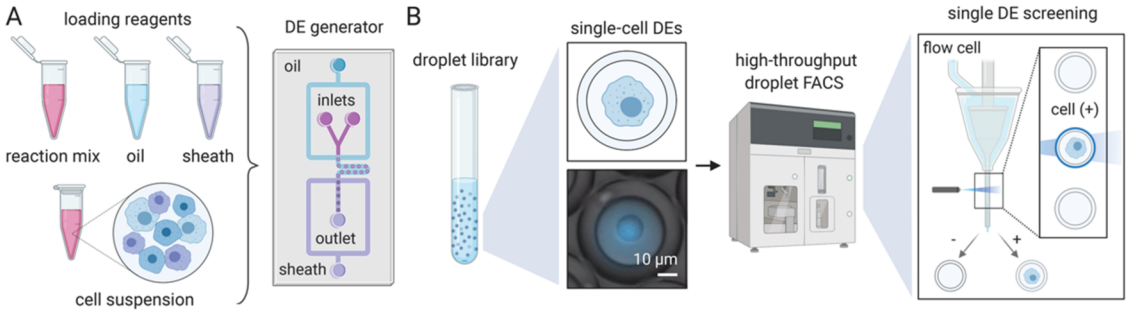

Figure 1. Schematic illustration of the Dropception workflow for cell encapsulation and droplet phenotyping. (A) DE picoreactors are generated from single-cell suspension and co-encapsulated with a reagent mixture in an oil shell surrounded by sheath buffer. (B) Droplet FACS is conducted on standard commercial flow cytometers at 12−14 kHz. The inset shows a mouse ES cell encapsulated in a DE droplet (Calcein AM, blue).

sequencing accuracy and depth.[20,21] Second, encapsulated cells could be isolated based on phenotypes not currently measurable with standard fluorescence-activated cell sorting[22] (FACS), such as enzymatic turnover, presence of secreted molecules, or quantification of proteins lacking cell surface markers.[11] Lastly, while droplets have been used to perform either single-cell phenotyping[23−25] (e.g., secreted marker screens, metabolite profiling, enzyme assays) or genome-wide sequencing[3,4,13,14] (e.g., RNA-seq, ATAC-seq, WGA), no technique combines the two for multiomic measurements. Sorting single droplets into individual wells of microwell plates by cell-derived biochemical signals with downstream genome-wide barcoding and profiling of the same cell would directly link cellular phenotypes to their underlying genetic mechanism.[3,4,10]

Most single-cell droplet assays employ water-in-oil (W/O) single emulsions in which a large (∼1 nL) aqueous droplet containing cells and reagents is surrounded by oil.[9] However, sorting these droplets can only be done via fluorescence-activated droplet sorting (FADS),[26,27] which requires extensive instrumentation, custom optics, and technical expertise to operate, severely limiting the applicability of the technique. As a result, there exists no easily accessible means to screen and sort droplets by cellular presence or functional response, preventing translation of powerful droplet-based sequencing technologies[3,4,14] to phenotypic multiomic profiling.

A promising alternative involves encapsulating cells within double emulsions (DE) (water−oil−water, W/O/W).[28] Unlike W/O droplets, DE droplets can be suspended in aqueous solutions, making them compatible with standard FACS instruments.[29] DEs have previously been combined with FACS for screening of bacterial or yeast mutant libraries.[25,30] However, these techniques suffer unpredictable cell occupancy and high multiple-cell loading ("multiplet") rates, confounding the downstream phenotype to genotype linkage. No prior effort has demonstrated successful encapsulation of large animal cells within picoliter-scale DE droplets, likely due to challenges associated with encapsulating large cells within droplets that are sufficiently small to pass through FACS nozzles without breakage and cross-contamination.[22]

Recently, we have developed a new method[31] (sdDE-FACS, for single droplet double emulsion FACS) to sort and recover large DE droplets via FACS by internal droplet fluorescence signals with similar performance to single-cell FACS (>70% sort recovery, 99% target sensitivity) using commercially available cytometers. Using sdDE-FACS, we established the first reliable isolation of single droplets based on fluorescence phenotype and recovered encapsulated nucleic acids at high efficiency post-sort.

Building on this progress, we present here the first demonstration of high-throughput FACS-based screening of picoliter-scale droplets containing single animal cells. Using a custom microfluidic device, we demonstrate a simple workflow, Dropception, for encapsulating large, complex cells (5−25 μm in diameter) within highly monodisperse DE droplets small enough (∼45 μm in total diameter) for FACS. We precisely tuned droplet size and cell concentration for an extremely high ratio of single- to multiple-cell loading events.[32] We benchmark performance of this technique across five standard mouse and human cell lines (Table S1) for robust encapsulation of single cells near maximal theoretical loading efficiency with no observable cell size bias. Using a modified sdDE-FACS workflow for large droplets, we screen tens of thousands of cell-containing DEs within minutes via a standard flow cytometer, establishing accurate discrimination of single-cell droplets from empty droplets. Finally, we apply Dropception to heterogeneous cell populations collected from a whole flatworm planarian, illustrating the wide applicability of this technique to a variety of cell types and primary samples.

MATERIALS AND METHODS

Device Fabrication and Preparation. The Dropception device was designed in AutoCAD 2019. Master molds and PDMS devices were fabricated via multilayer photolithography[33] and standard one-layer soft lithography, respectively. Device designs and protocols are available in the Supporting Information via an open-source repository.

Cell Preparation and Viability Measurement. Cells were cultured and dissociated according to ATCC standard protocols. Prior to droplet loading, cells were stained with Calcein AM UltraBlue (AAT Bioquest), resuspended in 0.04% (w/v) BSA-PBS solution, filtered with a 40 μm cell strainer, and diluted to a final calculated concentration of ∼2.5 M/mL with 20% OptiPrep density gradient medium (Sigma) as projected from culture measurements. Minor post-strain losses were observed for large cell lines. Viability and concentration measurements were conducted at multiple staging points via a Trypan Blue exclusion assay using a Countess cell counter (Life Technologies) (Table S2).

Double Emulsion Cell Encapsulation. An extensive step-by-step protocol describing the workflow is available in the Supporting Information. Picoliter DEs were generated using four syringe pumps (PicoPump Elite, Harvard Apparatus) for cell suspension and inner, oil, and outer sheath solutions. The inner phase was composed of 1× PBS with 0.5% BSA. The oil

https://dx.doi.org/10.1021/acs.analchem.0c02499
Anal. Chem. 2020, 92, 13262−13270

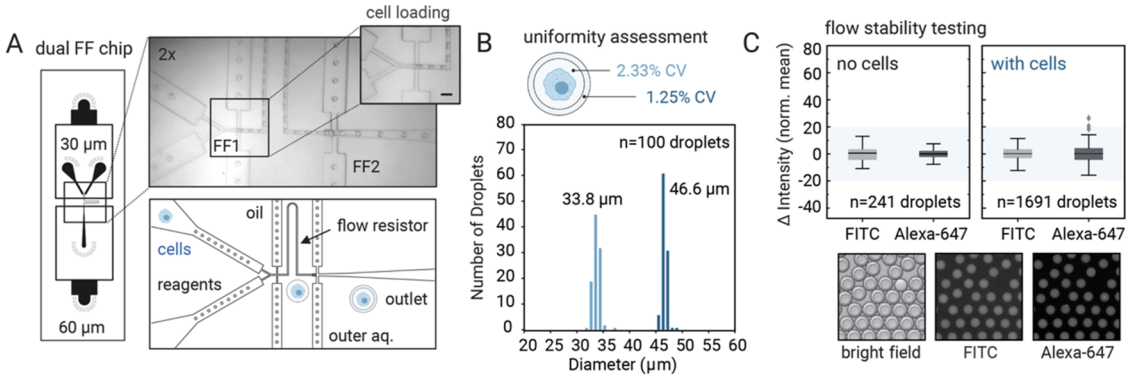

Figure 2. The Dropception device generates monodisperse droplets under stable flow. (A) Design and microscopy image of the device showing flow focuser features (FF1, FF2), inlets, channels, and outlet. Dimensions indicate relative channel heights of each flow focuser. Inset: cell loading at the inlet tree; flow line delineates relative volumetric contributions of inlets. Scale bar: 45 μm. (B) DE size characterization via microscopy denoting internal core (light blue) and total droplet (dark blue) diameters with corresponding coefficients of variation (CV) (n = 100, sample: mouse ES cell line, all cell lines shown in Figure S3). (C) Two-dye co-flow experiments with and without cells show flow stability across droplet populations; intensity is normalized to zero-mean (interquartile ranges: (−2.16, 2.68) and (−2.32, 2.21) for FITC; (−2.20, 1.95) and (−2.70, 2.82) for Alexa-647 in the absence and presence of cells, respectively).

phase was composed of HFE7500 fluorinated oil (Sigma) and 2.2% Ionic PEG-Krytox[34] (FSH, Miller-Stephenson). The carrier phase contained 1% Tween-20 (Sigma) and 2% Pluronic F68 (Kolliphor 188, Sigma) in PBS.[31] Each phase was loaded into syringes (PlastiPak, BD) and connected to the device via PE/2 tubing (Scientific Commodities). Relatively low flow rates (400:125:105:6000 μL/h, oil.cell/reagent/outer) were used to reduce cell shear stress.

Picoreactor Phenotyping via Flow Cytometry. Single-cell DE picoreactors were analyzed via FACS using the sdDE-FACS workflow.[31] Briefly, 100 μL of collected droplets in 500 μL of sheath buffer containing 1% Tween-20 (Sigma) in 1× PBS was analyzed on an SH800 flow cytometer (Sony) at 12 kHz using a standard 408 nm laser configuration and a 130 μm sorting nozzle. Droplet sorting rates were maintained below 1000 eps to achieve single droplet sort purity similar to single-cell FACS.[22] All FACS parameters are reported in Table S5.

RESULTS AND DISCUSSION

The Dropception Workflow. The Dropception workflow takes place in two stages (Figure 1): (1) encapsulation, in which cells and reagents are introduced into a one-step microfluidic device to yield a library of uniform, picoliter-scale DE droplets, and (2) screening, in which these DE droplets are passed through an FACS machine for high-throughput analysis by cellular presence or phenotype. To facilitate adoption of the technique, we employ a widely available commercial flow cytometer and our droplet generation device requires only four syringe pumps and an inexpensive benchtop microscope for operation (Table S3).

This workflow addresses several technical challenges required for high-throughput screening of cell-containing picoliter-scale droplets ("picoreactors"). First, double emulsions must be small enough for FACS yet large enough to encapsulate mammalian cells reliably[35] and must remain stable during droplet generation and flow cytometry.[29,31,36] Second, FACS must be able to accurately discriminate between cell-containing droplets and empty droplets and, ideally, associate fluorescence signals with encapsulated *single* cells.[3,4,14] Lastly, the workflow must be compatible with multiple cell types and in-droplet reaction schemes to facilitate translation and broad applications.[10]

To address these challenges, we designed a custom microfluidic device for large cell encapsulation into picoliter double emulsions capable of FACS analysis and sorting. By generating uniform droplets on a picoliter scale via a specific loading distribution (Poisson, λ < 0.05), we ensure that cell-containing droplets achieve high single-cell purity (>98% of cell-containing droplets are single cells) without compromising low reagent consumption, a common pitfall of large-droplet techniques.[32] Our workflow enables a variety of potential reaction schemes; picoliter droplet reactions using our one-step device can co-encapsulate lysis and reaction solutions for genomic and transcriptomic profiling, secreted marker analysis, or enzymatic turnover. Each experiment takes less than 30 min including cell staining, minimizing changes in the native state of encapsulated cells[37] (Figures S1, S2).

Device Design and Characterization. High data quality in single-cell analyses depends on the ability to discern which droplets contain single cells.[20,21] Previously, it has been difficult to attain predictable single-cell loading in DEs due to droplet polydispersity.[25,30] To achieve single-cell droplet FACS, picoliter DEs needed for FACS analysis must be highly uniform in size to yield accurate cell occupancy distributions.[32] However, monodisperse DE generation is technically challenging, especially when attempting to load large particles into small droplets.[28] To enable robust large cell encapsulation in small double emulsions, we designed a novel device containing optimized design elements for flow stability during large particle loading.

The Dropception device employs a dual flow-focusing geometry[38,39] for co-encapsulation of cells and assay reagents into picoliter-scale droplets (Figure 2A, Supporting Information). In the first flow focuser (FF1), cells and reagents from the inlet tree meet a stream of carrier oil and are encapsulated into regularly spaced W/O single emulsions. In the second flow focuser (FF2), the cell-laden single emulsions in their carrier oil meet an aqueous stream and are pinched off to form W/O/W double emulsion droplets, each containing an oil shell and aqueous interior. The carrier oil, HFE7500 with a 2.2% ionic Krytox surfactant, is a biocompatible fluorocarbon oil optimized for high oxygen delivery to encapsulated cells,[34,40] PCR stability,[36] and robust performance in DE flow cytometry.[31] Device operation requires only 100 μL of cell

https://dx.doi.org/10.1021/acs.analchem.0c02499
Anal. Chem. 2020, 92, 13262−13270

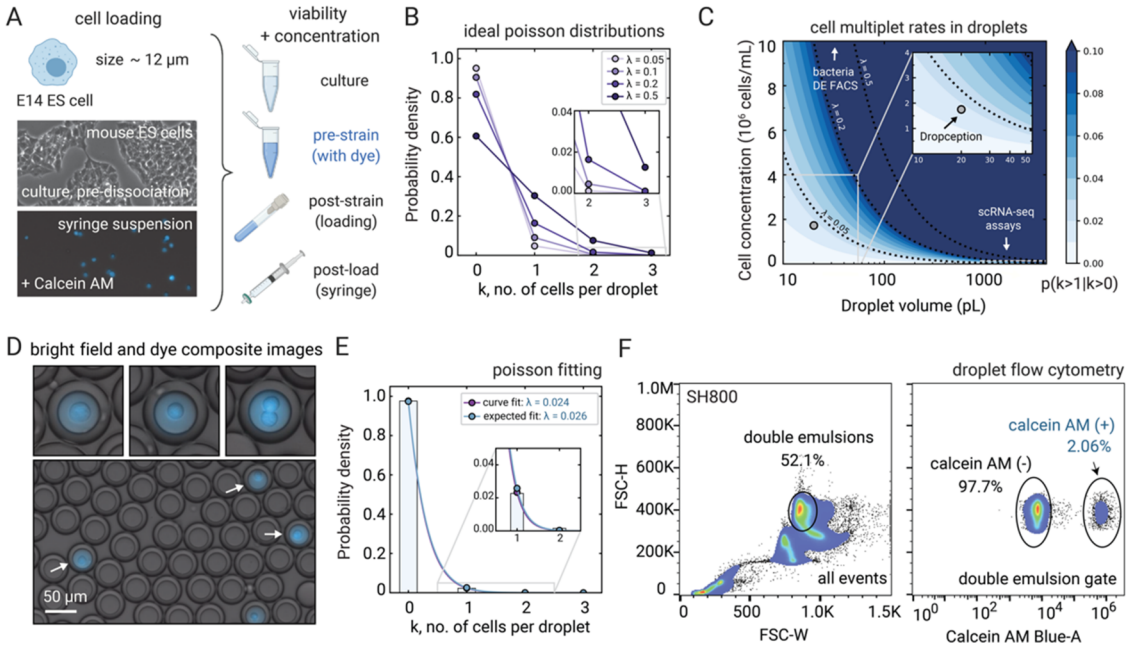

Figure 3. ES cell encapsulation approaches theoretical loading with single-cell DE discrimination by FACS. (A) Microscopy images show mouse E14 cells from culture and syringe suspension, with cartoons depicting additional concentration and viability measurement steps (Table S2). (B) Expected droplet occupancy distributions across modeled Poisson loading regimes by event rate (λ). (C) Multiplet loading probabilities (as a percentage of cell-containing droplets) under typical Poisson droplet encapsulation by cell concentration and droplet size; arrows highlight comparable technologies. The inset shows the low Poisson regime chosen for Dropception. (D) Microscopy images of loaded ES cells in DE droplets. Arrows indicate single-cell loading (the $k = 2$ inset shows a rare multiplet event). (E) Microscopy-determined cell occupancy fitted to a Poisson and plotted against expected distribution. The inset shows single versus doublet cell occupancy ($n = 7104$ droplets). (F) FACS analysis of DE droplets containing ES cells. DE-gated population (right) shows two clearly separable populations (cell containing (+) vs empty (−) droplets, $n = 45{,}000$ droplets).

suspension or reaction mix (compared to >1000 μL in techniques such as DropSeq[3]) with minimal reagent consumption per droplet, enabling screening of precious samples.

Upstream of the first flow focuser, we designed an inlet tree containing two wide channels without flow filters, each spaced 30° to normal, which funnel into short resistive elements to focus flow at a short channel (Figure 2A). The short resistive elements at the inlet tree have channel dimensions equivalent to the desired droplet core diameter; this design choice reduces cell-induced flow perturbations by metering large cells into the impending droplet junction at cell spacings that match subsequent droplet encapsulation volumes. At each flow focuser, additional short resistive elements produce ordered, triggered flow[41] where each aqueous single emulsion is encased in an oil emulsion to create a double emulsion at efficiencies beyond stochastic statistics (>99.9% of droplets contain a single emulsion core).

To minimize cross-contamination between droplets, the cell and reagent inlet channels meet just 110 μm before the FF1 nozzle (below distances typical for intersolution diffusion). During operation, cells are suspended in a density gradient medium (20% OptiPrep) to avoid settling in the loading syringe. In this region, the difference between the index of refraction of the cell solution and the reaction mix allows for clear delineation of the relative contributions of each inlet (inset, Figure 2A), thereby serving as a precise visual readout to tune relative reaction volumes in the droplet core during operation[42] (Supporting Information).

The Dropception device has channel heights and nozzle widths of 30 and 22.5 μm for the FF1 region and 60 and 45 μm for the FF2 region, respectively. Droplet generation with cell encapsulation produced DEs with diameters of 34 and 47 μm for the inner aqueous core and outer oil shell, respectively (20 and 54 pL by volume) (representative population, Figure 2B). Matching the flow rate of the outer aqueous sheath to the periodicity of single emulsion generation yielded highly monodisperse DE populations with uniform inner aqueous core sizes (2.33 and 1.25% CV on the inner core and outer shell diameters, respectively; Figure 2B). These results were consistent across all subsequent data presented here (Figures 4, 5, Figure S3) using a single set of flow conditions (Table S4).

To assess the uniformity of flow from each inlet during device operation, we introduced FITC- and Alexa-647-conjugated BSA into the cell and reagent inlets, respectively, and compared the variance in dye intensity distributions in the presence and absence of cells (Figure 2C). Alexa-647 and FITC fluorescence intensity distributions associated with each droplet were narrow in both cell and cell-free conditions (Figure 2C), demonstrating steady, nonpulsatile flow from each inlet. Combined, these data indicate robust operation of the Dropception device for stable droplet generation, even under large cell loading in highly constrained channels.

Single-Cell Encapsulation of Mouse Embryonic Stem Cells. As a first application of the Dropception device and workflow, we encapsulated mouse embryonic stem (ES) cells (ATCC: E14 cell line) (Figure 3A, Video S1). ES cells are a critical cell line for investigating pluripotency and stemness,[43] profiling transcriptional and epigenomic reprogramming,[44] and are a vector for synthetic biology studies.[45] Mouse ES cells are also relatively small (11−13 μm diameter, 1.5 pL volume) with

https://dx.doi.org/10.1021/acs.analchem.0c02499
Anal. Chem. 2020, 92, 13262−13270

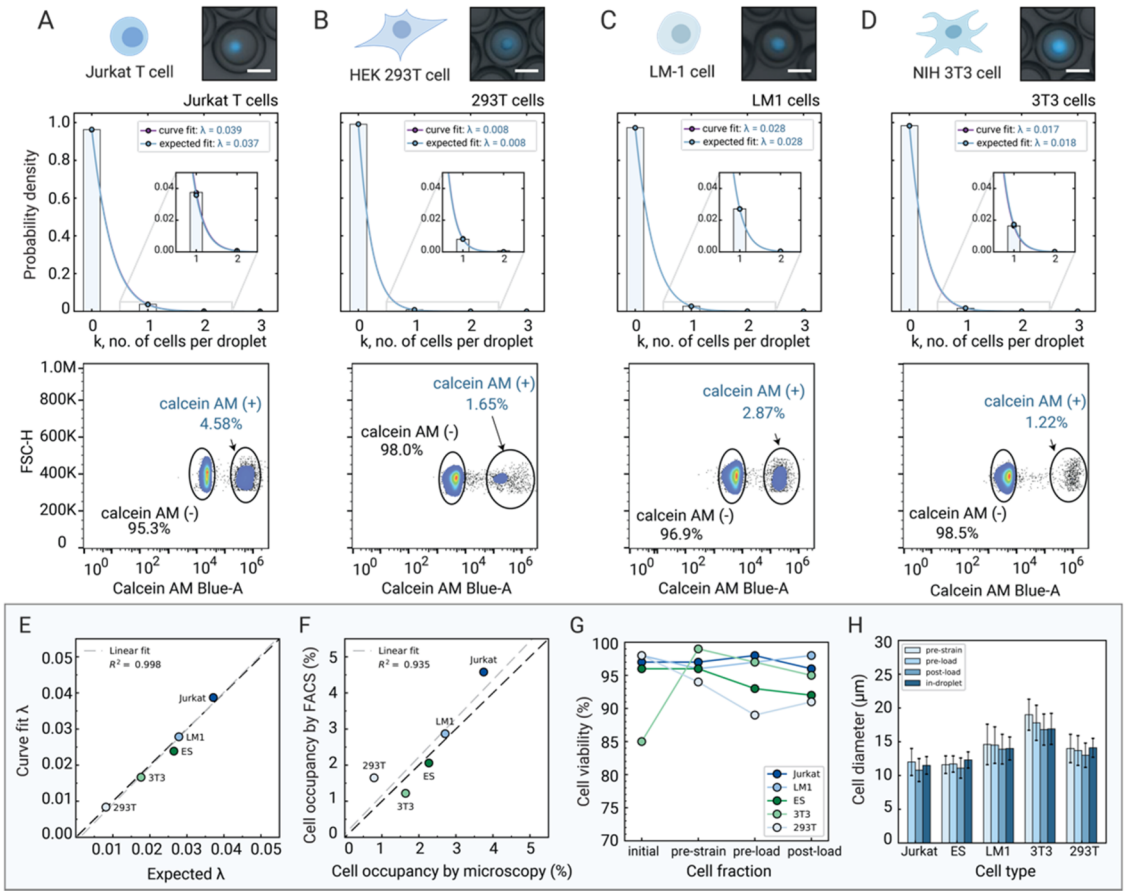

Figure 4. Benchmarking single-cell encapsulation and phenotyping of Jurkat T, HEK 293T, LM-1, and 3T3 cell lines in DE droplets. (A–D) Microscopy images (top), cell occupancy distributions (middle) (n = 4028–7449 droplets), and FACS phenotyping (bottom) (n = 45,000 droplets) of the four cell lines in DE picoreactors. Scale bars: 25 μm. (E) Fitted versus expected event parameter for Poisson loading across all cell lines. (F) Cell occupancy determined by FACS plotted against single-cell occupancy determined by microscopy counts. Dashed gray lines depict linear fits. (G) Cell viability measurements during processing steps in the cell encapsulation workflow, including suspension post-loading. (H) Cell diameters as measured during the workflow or within droplet volume across all cell lines.

uniform morphology, providing a convenient experimental system to test cell encapsulation efficiency in picoliter-scale droplets (Figure S4).

Single-cell droplet encapsulation should follow a typical Poisson distribution for stochastic loading[32] (Figure 3B)

$$P(k) = \frac{\lambda^k e^{-\lambda}}{k!} \tag{1}$$

where k is the number of cells within each droplet and λ (mean number of cells per droplet) is the event rate, as given by

$$\lambda = CV_dQ_f \tag{2}$$

where C is the loading concentration of cells (cells/pL), V_d is the volume of the droplet (pL), and Q_f is the fraction of volumetric flow contributed by the cell suspension.

For most single-cell droplet techniques, the large majority of droplets are empty with only a small proportion containing one or more cells. Many single-cell droplet techniques optimize for single-cell occupancy ($P(k = 1)$) over empty droplets ($P(k = 0)$), at the expense of a high proportion of droplets containing two or more cells (Figure 3B,C). This fractional occupancy can be controlled by selection of droplet size and loading concentration of cells (Figure S5A,B). Prior techniques using picoliter DEs that encapsulate yeast or bacteria at high concentration estimate up to 50% of droplets contain single cells ($\lambda > 0.5$).[25,30] However, these techniques suffer extremely high multiplet rates (>10%), preventing true single-cell resolution in downstream sequencing.

While some mammalian cell techniques (e.g., DropSeq,[3] Indrops,[4] 10X[14]) reduce multiple-cell loading events for sequencing accuracy, extremely low cell loading concentrations are required (Figure 3C) and therefore reagent consumption (e.g., reverse transcription enzymes, reaction components) is high to balance volumetric demands of the large droplet size. As a result, these widely adopted sequencing technologies strike a compromise between increasing overall costs to achieve single-cell purity and reducing data quality by tolerating multiplets (~4–6% multiplet rate; inset, Figure S5C).

Here, we chose to perform single-cell encapsulation under a Poisson distribution with a very low event rate ($\lambda < 0.05$) via explicit selection of droplet size (~35 μm, aqueous core) and cell loading concentrations (0.5–2.5 × 10^6 cells/mL). Cell occupancies are expected to be 1–5% under this distribution (Figure 3B). Of droplets containing cells, a minimum of 98% should contain only a single cell. Thus, this operating regime allows higher single-cell purity in the cell-containing droplet population via small droplet volumes (Figure 3C).

To assess cell encapsulation efficiency using our workflow, we loaded ES cells into double emulsions (Figure 3D). We

https://dx.doi.org/10.1021/acs.analchem.0c02499
Anal. Chem. 2020, 92, 13262–13270

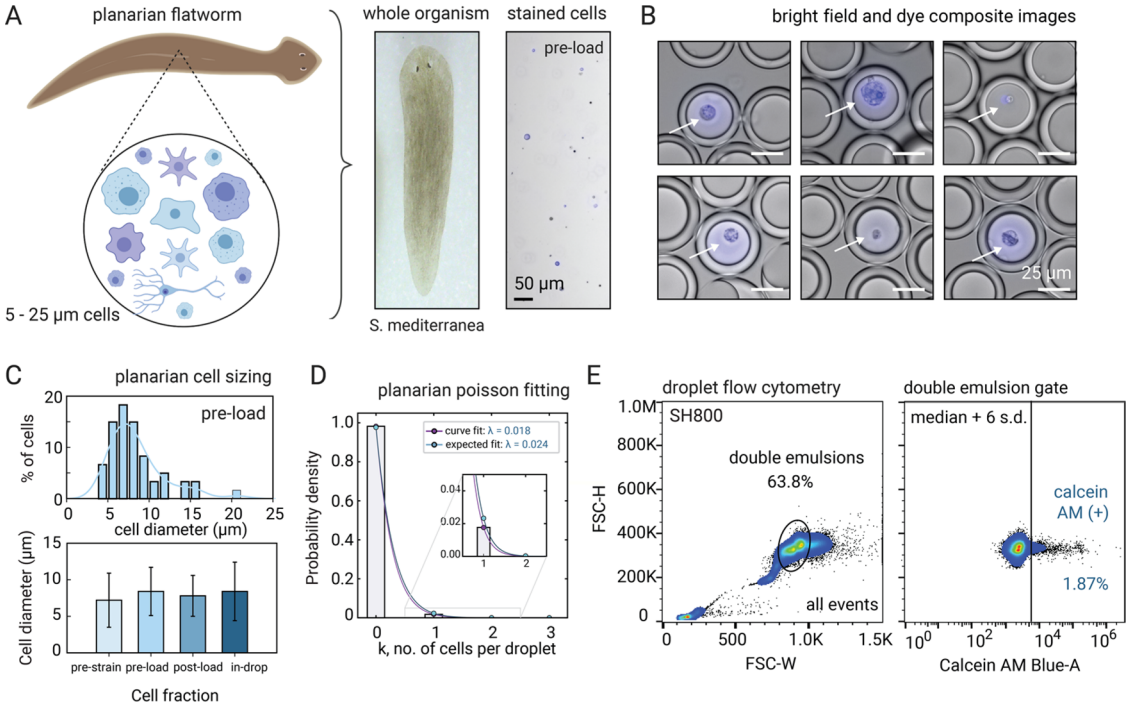

Figure 5. Single-cell DE encapsulation of dissociated planarian cells suggests robust applicability to heterogeneous primary tissue. (A) Illustration and microscopy images of complex cell populations in the planarian (Calcein AM, blue). (B) Representative microscopy images of *S. mediterranea* cells in DE droplets highlighting size variance of the encapsulated population. (C) Cell size distributions across workflow steps show broad variation in the pre-loaded cell fraction (top), with similar variance observed in droplet-loaded cells (bottom). (D) Microscopy-derived cell occupancy with Poisson fits. (E) FACS screening of DEs containing planarian cells (n = 43,238 droplets).

performed manual microscopy counts of cellular occupancy across thousands of droplets and fit these data to a Poisson distribution (curve fit, Figure 3E). Given known cell concentrations and droplet volume, we compared our data to ideal Poisson loading (expected distribution, Figure 3E). Single-cell occupancies between the predicted and measured distributions agreed well ($P(k = 1)$; 2.27% measured, 2.58% expected), with closely corresponding event rates within the intended low λ operating regime (λ: 0.024 curve fit; 0.026 expected), establishing optimal performance of cell loading near theoretical maximal loading efficiency.

Single-Cell Picoreactor Screening. Next, we investigated whether we could discriminate cell-containing droplets from empty droplets via high-throughput DE FACS. Using a Sony SH800S FACS instrument and settings from our sdDE-FACS pipeline[31] (Table S5), we analyzed tens of thousands of cell-laden DE droplets (Figure 3F). DEs comprised >50% of recorded events under low scatter thresholds that show small dust, free oil, and other debris, demonstrating high sample integrity with little evidence of droplet breakage.[31] To the best of our knowledge, this represents the first time that droplets this large (45−48 μm) have been analyzed via FACS.

To assess whether cells encapsulated within DEs could be reliably detected via their Calcein AM fluorescence signals, we gated DE events based on their forward scatter signals (FSC-H vs FSC-W, typical of large particle analysis[22]) and examined the fluorescence intensities of the gated population. Analysis of the DE gated population revealed two clearly separable populations with ∼100-fold higher intensities associated with cell-containing droplets (median population intensities of 5.49 × 10^3 vs 4.43 × 10^5). Across the total population of droplets, 2.06% was identified as containing cells (Figure 3F).

This conservative FACS estimate of cellular occupancy agrees well with a microscopy-derived single-cell occupancy of 2.27%. Under the fitted Poisson distribution from empirical cell occupancies (λ = 0.024), 98.8% of cell-containing droplets should be single cells, with 1.2% remaining as multiplets in this sample. Combined, these findings suggest that picoliter DE encapsulation in a low Poisson regime (λ < 0.05) allows for high-throughput methods of analysis such as FACS to accurately assign phenotypes during droplet screening.

Systematic Benchmarking across Four Standard Cell Lines. Next, we probed the experimental limits of Dropception by testing the ability to encapsulate and phenotype four additional standard cell lines with a wide range of morphologies and sizes (5−20 μm) (Table S1, Figures S3, S4): human T lymphocytes and mouse macrophage cells (Jurkat and LM-1, respectively; key model systems for immunological studies[46]), human embryonic kidney cells (HEK 293T, common vectors for synthetic biology[47]), and mouse embryonic fibroblasts (NIH 3T3, an important resource across cancer studies[48]). Similar to ES cell loading, we systematically quantified single-cell DE droplet occupancies using both microscopy and FACS.

Microscopy established successful encapsulation of all four cell lines (Figure 4). As before, cellular occupancies (4000 droplets/condition) were well-fit by a Poisson distribution and in agreement with expectations given observed droplet size and loading concentration for all four cell lines (R^2 = 0.998) (Figure 4A−D). This agreement demonstrates consistent performance approaching theoretical loading efficiency, even for large and morphologically diverse cell types (e.g., 293T and 3T3), and suggests an absence of common experimental pitfalls to cell loading such as cell clumping, flow instability, or steric bias. We found that the same flow rates could be used for

https://dx.doi.org/10.1021/acs.analchem.0c02499
Anal. Chem. 2020, 92, 13262−13270

efficient loading of all cell lines, suggesting that this pipeline may be used without adjustment for a variety of different samples and enhancing overall translatability (Table S4).

Upon screening each of the four DE-loaded cell lines via FACS (Figure 4), we observed clearly separable Calcein AM fluorescence intensities for gated DE populations, corresponding to empty and cell-containing droplets. For all cell types, the percentage of cell-containing droplets recorded with FACS showed excellent agreement with single-cell occupancy determined by manual microscopy inspection (R^2 = 0.935, Figure 4F). Across all samples, we observed only a minor discrepancy in estimated loading rates (0.79 vs 1.65% for microscopy vs FACS) for HEK293T cells, likely because their relatively large size caused them to settle during FACS loading.

Finally, we characterized additional metrics of workflow performance including viability (Figure 4G,H) and cell size variation (Figure 4H) at all stages pre- and post-load. For all cell lines, viability remained >85% over the entire 30 min processing window, with expected small increases in viability after filtering and pelleting to remove dead cells and debris. High cell viability during loading results in fewer free-floating nucleic acids and debris from cellular death, minimizing single-cell picoreactor cross-contamination. We observed no significant cell size distribution changes upon droplet loading even in large cell types (Figure 4H), indicating an absence of steric constraint for large cell (1−3 pL) loading into 20 pL DEs.

Application to a Whole Flatworm. Single-cell encapsulation in emerging droplet screening assays has largely been demonstrated using cultured cell lines, which are uniform in cell size and morphology.[2] However, a critical question in the field is whether new microfluidic strategies are compatible with heterogeneous cell populations freshly isolated from whole animals or tissue dissection.

To evaluate the applicability of Dropception for primary tissue, we encapsulated single cells dissociated from whole planarian flatworms (Figure 5A). Planarians contain a large pool of pluripotent stem cells (neoblasts) and possess exceptional and unremitting regenerative capacity throughout their entire body, providing a powerful biological system for in vivo stem cell studies.[49,50] However, planarians are not amenable to most cell probing assays, such as transgenic marker integration or cell surface antibody markers,[51] and thus, nonmodel organism research would benefit immensely from the ability to FACS-isolate cells by droplet-accessible phenotype (e.g., genomic PCR and secretory protein analysis).[50] Furthermore, planarians have a sticky outer mucosal layer and comprise hundreds of unique cell types that vary widely in size (5−25 μm), morphology, and cellular biology,[19] posing a challenge for droplet encapsulation.

Following the same workflow as for cultured cells, we performed a fresh dissociation of whole planarians and loaded the resultant cell suspension into the Dropception device (Figure 5). Despite the anticipated challenges, we achieved robust single-cell encapsulation of diverse cell sizes and morphologies (Figure 5B). Cell size distributions of dissociated primary cells as measured before loading ("pre-load") and in the remaining syringe suspension after loading ("post-load") were recapitulated in loaded droplets (Figure 5C), confirming that loading efficiencies are not biased by cell size even for heterogeneous cell populations. Importantly, droplet counts obtained from microscopy revealed that planarian single-cell occupancy in DE picoreactors was near theoretical limits (1.77%) (Figure 5D).

FACS DE analysis revealed clearly discernable populations of empty and cell-containing droplets with 1.87% cell loading, in agreement with microscopy (Figure 5E). Flow cytometry gates for this sample were placed conservatively by comparison to negative droplet populations (median fluorescence intensity of the Calcein AM channel (MFI: 2302) + 6 s.d. (robust s.d.: 551), consistent with empty droplet gates of cell line experiments. Broad fluorescence signals relative to prior cell line data likely stem from variable dye uptake in primary cells as only ∼60% of planarian cells exhibit bright Calcein AM staining (Figure S6). Under the theoretical cell encapsulation distribution for this sample (λ = 0.024), single cells should account for 98.8% of all cell-containing droplets, suggesting minimal multiple-cell bias during future downstream genomic processing from droplets.

CONCLUSIONS

In this work, we present a novel method capable of high-throughput phenotyping of large animal cells within double emulsion picoreactors compatible with FACS. Double emulsions produced with our workflow are uniform, highly monodisperse, and stable under cell loading. In all cell lines, single-cell occupancy determined via microscopy approached maximal efficiency of ideal Poisson loading with no observed cell size bias. Importantly, droplet cell occupancies reported by high-throughput FACS mirror those calculated from microscopy, establishing that FACS can be used to screen droplets at single-cell resolution. Encapsulation of primary cells from a whole planarian flatworm, a complex organism with high cellular diversity and technical challenges associated with sample preparation, performed as well as uniform cell lines.

Unlike other droplet sorting strategies,[26,52] Dropception achieves higher throughput and requires only commercially available equipment and limited technical expertise, making the technology easily adoptable by bioscience labs (Table S6). For single-cell encapsulation, only an inexpensive microscope and syringe pumps are needed to operate the Dropception device; the setup is easy to use and can be assembled within a day. Downstream, we demonstrate high-throughput DE screening using a widespread, inexpensive benchtop flow cytometer (Sony SH800). We have previously established that DE droplets can also be sorted using BD FACS Aria II and III machines[31] and similarly anticipate that Dropception will be compatible with most FACS instruments.

Furthermore, the Dropception pipeline reduces shear stresses on sorted cells via droplet shielding during FACS,[53] minimizing changes in underlying cell biology. The time required to load cells is short (<30 min) and cells can be immediately lysed (and thus cell state "frozen") upon encapsulation (Figure S7), enhancing the likelihood that recovered phenotypes accurately reflect the native cell state.[37] Moreover, our unique device geometry allows for low flow rates and small droplet volumes, conserving samples and thus enabling new opportunities for single-cell analysis of precious samples, including clinical samples, nonmodel organisms, or cells under perturbation.

High-throughput screening and sorting of DE droplets containing complex animal cells open up a wide range of potential applications. Sorting and sequencing only cell-containing droplets could vastly reduce reagent costs[9] and increase accuracy for downstream next-generation sequencing,

https://dx.doi.org/10.1021/acs.analchem.0c02499
Anal. Chem. 2020, 92, 13262−13270

including eliminating common issues with single-cell droplet sequencing such as reads from empty droplets due to encapsulation of free-floating transcripts.[21] In addition, Dropception provides a method to screen cells based on a range of reaction- or secretion-based phenotypes traditionally inaccessible to FACS with enhanced sensitivity compared to other droplet techniques due to picoliter reaction volumes.[54]

In future work, we anticipate Dropception will facilitate a variety of multiomic assays on the same single cell[10] via isolation of single DE droplets for massively parallel downstream analysis (Figure S8). Using our prior sdDE-FACS pipeline for isolating individual DEs and performing downstream plate-based PCR reactions,[31] single-cell droplets of a particular phenotype generated via the Dropception workflow could be sorted into wells of a multiwell plate for genome-wide processing, thereby diluting droplet buffers ∼100,000-fold and thus enabling multiple assays per cell without a need for buffer exchange. Coupling genomic, epigenomic, or transcriptomic profiling in plates to in-droplet cellular phenotyping with this potential scheme would allow direct investigation of genetic mechanisms driving cellular functions in the same cell using only simple plate-processing workflows. In this way, Dropception would expand the current repertoire of nucleic acid single-cell droplet assays to include functional analysis, perturbation screening, or multiomic profiling by coupling the throughput of droplet microfluidics with the power of flow cytometry.

■ ASSOCIATED CONTENT

Supporting Information

The Supporting Information is available free of charge at https://pubs.acs.org/doi/10.1021/acs.analchem.0c02499.

Extended methods; a full step-by-step workflow protocol; schematic overview of assay runtime; droplet monodispersity measurements across all cell lines; representative cell culture images of each cell line and representative large field-of-view image of droplet encapsulation; singlet rates, multiplet rates, and cell occupancies under modeled Poisson loading regimes for single-cell droplet encapsulation; FACS analysis of cell-stain uptake of planarian cells from primary dissociation; lysis buffer demonstration with DE droplets; multiomic reaction scheme; cell lines used in this study; concentration and viability measurements of all cell lines; Dropception droplet generation setup components and cost; flow rates used for all ATCC cell lines; FACS gates and parameters; comparison of single and double emulsion techniques (PDF)

Single-cell encapsulation of mouse ES cells in double emulsion picoreactors (MOV)

■ AUTHOR INFORMATION

Corresponding Authors

Bo Wang − *Department of Bioengineering and Department of Developmental Biology, Stanford University, Stanford, California 94305, United States*; Email: wangbo@stanford.edu

Polly M. Fordyce − *Department of Bioengineering, Chem-H Institute, and Department of Genetics, Stanford University, Stanford, California 94305, United States; Chan Zuckerburg BioHub, San Francisco, California 94158, United States;* orcid.org/0000-0002-9505-0638; Email: pfordyce@stanford.edu

Authors

Kara K. Brower − *Department of Bioengineering and Chem-H Institute, Stanford University, Stanford, California 94305, United States*

Margarita Khariton − *Department of Bioengineering, Stanford University, Stanford, California 94305, United States*

Peter H. Suzuki − *Department of Bioengineering, Stanford University, Stanford, California 94305, United States*

Chris Still, II − *Institute for Stem Cell Biology and Regenerative Medicine, Stanford University, Stanford, California 94305, United States*

Gaeun Kim − *Department of Bioengineering, Stanford University, Stanford, California 94305, United States*

Suzanne G. K. Calhoun − *Department of Chemical Engineering, Stanford University, Stanford, California 94305, United States*

Lei S. Qi − *Department of Bioengineering, Chem-H Institute, and Department of Chemical and Systems Biology, Stanford University, Stanford, California 94305, United States*

Complete contact information is available at: https://pubs.acs.org/10.1021/acs.analchem.0c02499

Author Contributions

◆K.K.B. and M.K. contributed equally. This work was completed with contributions from all authors. K.K.B., M.K., B.W., and P.M.F., wrote the manuscript, with input from all authors. All authors have given approval to the final version of the manuscript.

Notes

The authors declare the following competing financial interest(s): Methods and techniques outlined in this work are disclosed in a U.S. patent filing, U.S. PTO Application No. 62/693,800, filed by co-authors K.K.B and P.M.F.

The device design, software resources, and data are available via an Open Science Framework repository at DOI 10.17605/OSF.IO/H4SR9.

Methods and techniques outlined in this work are disclosed in a U.S. patent filing, U.S. PTO Application No. 62/693,800, filed by co-authors K.K.B. and P.M.F.

■ ACKNOWLEDGMENTS

The authors acknowledge members of the Fordyce and Wang laboratories for their feedback. We acknowledge Dr. David Sukovich and Dr. Adam Abate (UCSF) for sharing their flow-focusing device design, which was modified to include new design elements in this study. Figure elements in this work were produced with Biorender Scientific Illustration software. This work was supported by an NIH grant 1DP2GM123641 (P.M.F.) and an HFSP grant RGY0085/2019 (B.W.). K.K.B. acknowledges support as a Chem-H CBI fellow (NIHT32 GM 120007) and a Siebel Scholar. M.K. acknowledges support as a BioX SIGF Lavidge and McKinley fellow. P.M.F. is a Chan Zuckerberg Biohub Investigator.

■ ABBREVIATIONS

FACS fluorescence-activated cell sorting
DE double emulsion

REFERENCES

(1) Svensson, V.; Vento-Tormo, R.; Teichmann, S. A. *Nat. Protoc.* **2018**, *13*, 599−604.
(2) Yuan, G.-C.; et al. *Genome Biol.* **2017**, *18*, 84.
(3) Macosko, E. Z.; et al. *Cell* **2015**, *161*, 1202−1214.
(4) Klein, A. M.; et al. *Cell* **2015**, *161*, 1187−1201.
(5) Buenrostro, J. D.; et al. *Nature* **2015**, *523*, 486−490.
(6) Achim, K.; et al. *Nat. Biotechnol.* **2015**, *33*, 503−509.
(7) Battich, N.; Stoeger, T.; Pelkmans, L. *Nat. Methods* **2013**, *10*, 1127−1133.
(8) Alemany, A.; Florescu, M.; Baron, C. S.; Peterson-Maduro, J.; van Oudenaarden, A. *Nature* **2018**, *556*, 108−112.
(9) Zhang, X.; et al. *Mol. Cell* **2019**, *73*, 130−142.e5.
(10) Stuart, T.; Satija, R. *Nat. Rev. Genet.* **2019**, *20*, 257−272.
(11) Wen, N.; et al. *Molecules* **2016**, *21*, 881.
(12) Lan, F.; Demaree, B.; Ahmed, N.; Abate, A. R. *Nat. Biotechnol.* **2017**, *35*, 640−646.
(13) Lareau, C. A.; et al. *Nat. Biotechnol.* **2019**, *37*, 916−924.
(14) Zheng, G. X. Y.; et al. *Nat. Commun.* **2017**, *8*, 14049.
(15) Shahi, P.; Kim, S. C.; Haliburton, J. R.; Gartner, Z. J.; Abate, A. R. *Sci. Rep.* **2017**, *7*, 44447.
(16) Stoeckius, M.; et al. *Nat. Methods* **2017**, *14*, 865−868.
(17) Karaiskos, N.; Wahle, P.; Alles, J.; Boltengagen, A.; Ayoub, S.; Kipar, C.; Kocks, C.; Rajewsky, N.; Zinzen, R. P. *Science* **2017**, *358*, 194−199.
(18) The Tabula Muris Consortium. *Nature* **2018**, *562*, 367−372.
(19) Fincher, C. T.; Wurtzel, O.; de Hoog, T.; Kravarik, K. M.; Reddien, P. W. *Science* **2018**, *360*, eaaq1736.
(20) DePasquale, E. A. K.; et al. *Cell Rep.* **2019**, *29*, 1718−1727.e8.
(21) Lun, A. T. L.; Riesenfeld, S.; Andrews, T.; Gomes, T.; Marioni, J. C. *Genome Biol.* **2019**, *20*, 63.
(22) Shapiro, H. M. *Practical Flow Cytometry*, 4th ed.; Wiley-Liss: New York, 2003.
(23) Dhar, M.; et al. *Proc. Natl. Acad. Sci.* **2018**, *115*, 9986−9991.
(24) Chokkalingam, V.; et al. *Lab Chip* **2013**, *13*, 4740−4744.
(25) Aharoni, A.; Amitai, G.; Bernath, K.; Magdassi, S.; Tawfik, D. S. *Chem. Biol.* **2005**, *12*, 1281−1289.
(26) Baret, J.-C.; et al. *Lab Chip* **2009**, *9*, 1850−1858.
(27) Mazutis, L.; et al. *Nat. Protoc.* **2013**, *8*, 870−891.
(28) Chong, D.; et al. *Microfluid. Nanofluid.* **2015**, *19*, 1071−1090.
(29) Lim, S. W.; Abate, A. R. *Lab Chip* **2013**, *13*, 4563−4572.
(30) Ma, F.; Xie, Y.; Huang, C.; Feng, Y.; Yang, G. *PLoS One* **2014**, *9*, No. e89785.
(31) Brower, K. K.; et al. *Lab Chip* **2020**, 2062.
(32) Collins, D. J.; Neild, A.; deMello, A.; Liu, A.-Q.; Ai, Y. *Lab Chip* **2015**, *15*, 3439−3459.
(33) Brower, K.; White, A. K.; Fordyce, P. M. *JoVE* **2017**, *119*, 55276.
(34) Holtze, C.; et al. *Lab Chip* **2008**, *8*, 1632−1639.
(35) Hümmer, D.; Kurth, F.; Naredi-Rainer, N.; Dittrich, P. S. *Lab Chip* **2016**, *16*, 447−458.
(36) Sukovich, D. J.; Lance, S. T.; Abate, A. R. *Sci. Rep.* **2017**, *7*, 39385.
(37) Nguyen, Q. H.; Pervolarakis, N.; Nee, K.; Kessenbrock, K. *Fron.t Cell Dev. Biol.* **2018**, *6*, 108.
(38) Abate, A. R.; Thiele, J.; Weitz, D. A. *Lab Chip* **2011**, *11*, 253−258.
(39) Kim, S. C.; Sukovich, D. J.; Abate, A. R. *Lab Chip* **2015**, *15*, 3163−3169.
(40) Chen, F.; et al. *Anal. Chem.* **2011**, *83*, 8816−8820.
(41) Chabert, M.; Viovy, J.-L. *Proc. Nat. Acad. Sci.* **2008**, *105*, 3191−3196.
(42) Gerver, R. E.; et al. *Lab Chip* **2012**, *12*, 4716−4723.
(43) Jiang, N.; et al. *Thyroid* **2010**, *20*, 77−84.
(44) Incarnato, D.; Neri, F. *Genom. Data* **2015**, *3*, 6−7.
(45) Liu, Y.; et al. *Cell Stem Cell* **2018**, *23*, 758−771.e8.
(46) Abraham, R. T.; Weiss, A. *Nat. Rev. Immunol.* **2004**, *4*, 301−308.
(47) Kim, H.; Bojar, D.; Fussenegger, M. *Proc. Natl. Acad. Sci.* **2019**, *116*, 7214−7219.
(48) Montano, M. Model Systems. In *Translational Biology in Medicine*; Elsevier, 2014; pp. 9−33, DOI: 10.1533/9781908818652.9.
(49) Newmark, P. A.; Alvarado, A. S. *Nat. Rev. Genet.* **2002**, *3*, 210−219.
(50) Rink, J. C. *Dev. Genes Evol.* **2013**, *223*, 67−84.
(51) Alvarado, A. S.; Tsonis, P. A. *Nat. Rev. Genet.* **2006**, *7*, 873−884.
(52) Cole, R. H.; et al. *Proc. Natl. Acad. Sci.* **2017**, *114*, 8728−8733.
(53) Chen, Y.; Liu, X.; Zhang, C.; Zhao, Y. *Lab Chip* **2015**, *15*, 1255−1261.
(54) Streets, A. M.; Huang, Y. *Curr. Opin. Biotechnol.* **2014**, *25*, 69−77.

https://dx.doi.org/10.1021/acs.analchem.0c02499
Anal. Chem. 2020, 92, 13262−13270